Visnyk NTUU KPI Seriia – Radiotekhnika Radioaparatobuduvannia, 2017, Iss. 70, pp. 62–71

УДК 535.215.5

Engineering of Nanostructured Plasmonic Substrates for Use as SERS Sensors

Bandeliuk, O. V.[1,2], *Kolobrodov, V. H.*[2]

[1]University of Maine, France
[2]National Technical University of Ukraine "Igor Sikorsky Kyiv Polytechnic Institute", Ukraine

E-mail: *alex20bend@gmail.com*

Plasmonic nanostructures strongly localize electric fields on their surfaces via the collective oscillations of conducting electrons under stimulation by incident light at certain wavelength. Molecules adsorbed onto such surfaces experiences a strongly enhanced electric field due to the localized surface plasmon resonance (LSPR), which amplifies the Raman scattering signal from these molecules. This phenomenon is referred to as surface enhanced Raman scattering (SERS). Further enhancements in the Raman intensity have been achieved by designing plasmonic nanostructures with a controlled size, shape, composition, and arrangement. This review paper focuses on the theory and analyses the influence of protective coating with oxide materials an isolated plasmonic metal nanostructures. Starting with a brief description of the basic principles underlying LSPR and SERS, we compare two plasmonic metals, two dielectric materials and the effect of changing individual parameters of the nanostructure on output enhanced Raman signal.

Key words: SERS; plasmon; molecule; hetero transition metal-dielectric; nanostructure

Introduction

Surface-enhanced Raman scattering (SERS)

For a direct, label free and non destructive characterization of molecules, vibrational spectroscopes are efficient interesting techniques. Based on the determination of molecular or crystalline vibrations, Raman scattering provides many information about the studied object whatever is its nature (liquid, solid or gas). It enables the description of the chemical composition (atomic composition and chemical group) and structure (geometry, conformation...) of almost any kind of molecules or crystal [1]. However, Raman scattering is known to present a weak cross section meaning that only a weak part of the incident energy will be effectively scattered inelastically by the observed object. The Raman signal is thus very low($\approx 10^{-30} cm^2$) compared to others spectroscopies such as fluorescence or infrared spectroscopies. Thus, it is necessary to use a large quantity of matter to collect exploitable Raman signals. Typically, to study proteins in liquid phase for example, a concentration higher than 10^{-4} mol L^{-1} is required to obtain sufficient Raman signal with acceptable signal to noise ratio. For lower concentrations, it is necessary to increase the electromagnetic field around the target molecule. One way is to add nanostructured metallic film under irradiation and localized surface plasmon resonance (LSPR) at wavelength λ_{LSPR} will appear, meaning the appearance of surface waves corresponding to a collective oscillation of the excited conductive electrons or plasmons and local electromagnetic field will be induced. If molecules are deposited on or in the vicinity of the surface, the Raman signal will be enhanced. So detection of low concentrated molecules requires metallic surface nanostructure that promote enhanced Raman scattering (SERS).

Raman spectra are typically measured from monochromatic light source (laser) to excite the molecules. Scattered light then detected by a CCD camera. Scattered photons that lose energy are called Stokes scattering, and anti-Stokes scattering corresponds to photons that gain energy relative to the energy of the incident photon. The magnitude of the energy shift is called the Raman shift ($\Delta\omega$) and can be expressed by [2]:

$$\Delta\omega(cm^{-1}) = \left(\frac{1}{\lambda_0(nm)} - \frac{1}{\lambda_R(nm)}\right)\frac{(10^7 nm)}{(cm)} \quad (1)$$

Where λ_0 and λ_R are the wavelengths of the incident and Raman scattered beams, respectively.

The origin of SERS phenomenon is still not well understood but community agreed on the existence of two principal contributions: electromagnetic or plasmonic effect (ensemble of mechanisms leading to an enhancement of the electromagnetic field [3]) and chemical effect which encompasses phenomenons that generate the variation of polarisability of a probe molecule. It is admitted that contribution of the chemical effect would not exceed a factor 100 and thus

can be neglected in many casess compared to the electromagnetic effect that gives exaltation factor of 10^8 or even 10^{10} [1].

Electromagnetic effect include two distinct processes [1]. Creation of local electromagnetic field (E_{loc}) by plasmons. The enhancement factor F_{λ_0} can be expressed as:

$$F_{\lambda_0} = \left(\frac{E_{loc}(\lambda_{LSPR})}{E_{inc}(\lambda_0)} \right)^2 \quad (2)$$

Where E_{loc} is the enhance local field by the nanoparticle at the incident wavelength λ_0.

The second process results in the enhancement of the Raman scattered signal E_R from probe molecule (at λ_R) at the vicinity of the nanoparticle surface and it's called re-radiation process. The enhancement factor at the wavelength λ_R in this process is:

$$F_{\lambda_R} = \left(\frac{E_R(\lambda_R)}{E_{loc}(\lambda_{LSPR})} \right)^2 \quad (3)$$

So the final enhanced intensity I_{SERS} of the Raman signal scattered by the molecule can be written as:

$$I_{SERS} = F_{\lambda_0} F_{\lambda_R} I_0 \quad (4)$$

Where I_0 the Raman signal intensity scattered by the molecule.

If these two wavelengths λ_0 and λ_R are close to each other it is considered that this two factors are approximately equal. So SERS enhancement is at fourth power of the local enhancement of the electromagnetic field produced by the nanoparticle $I_{SERS} \approx [\frac{E_{loc}}{E_{inc}}]^4$. Hovewer, these two wavelengths (λ_0 and λ_R) can be separated by several tens on nanometers and, in this case, the wavelength shift between λ_0 and λ_R cannot be neglected. From the literature λ_{LSPR} should be located at some intermediate energy between the excitation λ_0 and Raman λ_R electromagnetic fields to provide the maximum enhancement of the two factors [1, 4].

The maximal enhancement factor (EF) can reach the value 10^{11} or even 10^{12} [5, 6] and can be calculated as [4]:

$$EF = \frac{[I_{SERS}/N_{surf}]}{[I_{NRS}/N_{vol}]} \quad (5)$$

Where N_{surf} is the number of molecules bound to the enhancing metallic substrate, I_{NRS} is normal Raman intensity and N_{vol} is number of molecules in the excitation volume.

1 Materials

1.1 Plasmonic Metals

Choice of the metal for use in SERS applications strongly depend on its optical properties.

If, for example, spherical metallic nanoparticle is illuminated with incident electromagnetic field E_{inc}, this leads to the appearance of an induced electric field $E_{Induced}$ around nanoparticle and this field can be expressed as:

$$E_{Induced} = \left(\frac{[\epsilon_m - \epsilon_d]}{[\epsilon_m + 2\epsilon_d]} \right) E_{inc} \quad (6)$$

Where ϵ_m is dielectric function of metal and ϵ_d is relative permitivity of the environment. This function is resonant while the real part of the dielectric constant of the metal $Re(\epsilon_m)$ is equal to $-2\epsilon_d$. In this case the enhancement of the surface plasmons increase the local field. For gold and silver this condition can be respected in visible part of the electromagnetic spectrum.

In its turn gold widely preferred to silver for biological applications for its relativey easier surface chemistry, the possibility of attaching molecules via thiol groups, good biocompatibility, and chemical stability [7].

The surface roughness of metallic films [8] or areal density of nanoparticles (NPs) [9, 10], shape of nanostructures [11] and environment around NPs (Equation 6) are a keys points to enhance the electromagnetic field for SERS measurements. About influence of the plasmonic metals shape on SERS activity we will talk in next paragraph.

2 Topology of gold nanostructures

Surface-enhanced Raman spectroscopy (SERS) depends on the highly intense localized electromagnetic fields (also known as "hot spots") produced by the process of surface plasmon resonance (SPR). In its turn, factors of SPR property are very sensitive to the parameters of plasmonic metallic nanoparticles including size, shape, morphology, distribution, and a surrounding environment.

Chemical synthesis is the most widely used method for preparing various kinds of plasmonic metallic structures, such as nanospheres, nanorods, nanocubes, nanostars [12–14]. However, using this approach it is difficult to control the distance and ordering of nanostructures in solution.

By far, the lithographic method is gaining popularity because it can give desired high-resolution, and its can be used to fabricate precisely controllable dimensions, interparticle spacing, and ordering of nanoparticles on substrates. There are different kinds of this technique such as electron beam lithography [15, 16], on-wire lithography [17] ,nanoimprint lithography, photolithography, laser interference lithography [2], etc.

Table 1 Influence of changing each design parameter (independently) on the system spectral response, while keeping the other parameters fixed, including the pitch (p x q) which is maintained to 300 x 300 nm^2 [18]. Where λ - resonant wavelength, T - transmittance, R - reflectance, A - absorbance.

Monopoles	Dipoles		Monopoles				Dipoles			
			λ	T	R	A	λ	T	R	A
90-130 nm	190-280 nm	length ↑	↑	↓	↑	↓	↑	↓	↑	∼
20-60 nm	4-44 nm	thickness ↑	↓	↓	↑	↓	↓	↑	↓	↓
10-40 nm	4-60 nm	width ↑	↓	↓	↑	∼	↓	↓	∼	↓
	4-44 nm	gap ↑					↓	↑	↓	↓

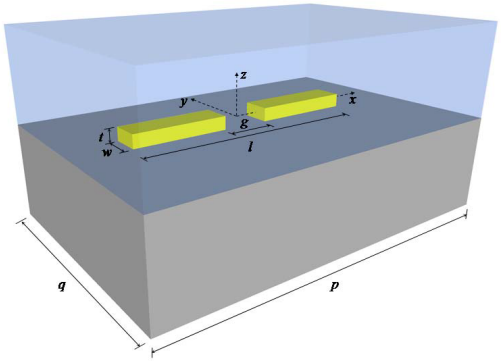

Fig. 1. Geometry of a unit cell of the system under study: an Au rectangular dipole antenna on a silicon substrate covered by water. An x-polarised plane wave source illuminates the antenna in the z-direction from the substrate [18].

The high degree of freedom available for such technique has enabled studies of the basic principles underlying electric field enhancements by well-designed metallic nanostructures. To find out the optimal topology of the nanostructure is the central question in SERS applications. Saba Siadat Mousavi et al [18] have been done a great work in determining the influence of length, width, thickness and gap of periodic rectangular gold nanomonopoles and nanodipoles on the transmittance, reflectance and absorptance response. In this work, infinite arrays of rectangular gold nanomonopoles and nanodipoles on a silicon substrate covered by water (Fig. 1) have been investigated extensively via 3D finite-difference-time-domain simulations (FDTD). Results of this paper gathered in Table 1.

Looking at Table 1 we can say that, for example, with increasing the length of the dipole from 190 to 280 nm, the resonant wavelength red-shifts, decreases the amount of power transmitted at resonance, and increases the level of reflectance of the system, but the absorptance remains almost unchanged.

To confirm that these simulations are right we can look at the work of Bryan F. Mangelson et al. [17]. Using on-wire lithography (OWL) they synthesized a composite plasmonic-semiconductor material composed of Au nanorod dimers embedded within anatase TiO_2 sheets. Optical properties of these structures can be tailored via the geometric control afforded by the OWL process to produce structures with various gap sizes exhibiting different electric field intensities near the surface of the metal particles. Spectra on (Fig. 2 a) were obtained by subtracting a solution containing only TiO_2 sheets as a background. It can be seen that as the gaps get larger the plasmon resonance of the structures blue-shift. The plots on (Fig. 2 b) show the intensity of the field at the resonances for each dimer, which are 1100, 1050, and 1030 nm, respectively. It is observed that as the gap becomes larger the electric field intensity decreases, showing the tunability available using this system. Additionally it can be seen that the electric field penetrates well into the semiconductor material. Electric field intensities are plotted on a log scale where zero is equal to the intensity of the incident field. So experimentally has been confirmed that the position of the dipole plasmon resonance shifts with increased coupling between rod segments as a result of the changing gap size.

In work Zhibing Zhan et al [11] have been fabricated, via a cost-effective nonlithographic route, perfectly ordered nanoparticle arrays with identical shape, uniform size and distance between these plasmonic gold nanoparticles on large-area substrates ($> cm^2$). Experimentally has been shown that with increasing the height (or in other words thickness) of nanopillar array we get a blue shift in resonant wavelength (Fig. 3). Also here excitation of multipole SPR modes will not necessarily result a peak broadening effect. In fact, the width of the SPR peak mainly involved in the uniformity of NPs, including size, shape and distribution in addition to the multipole excitation. Increasing heights strengthened the restoring force to the displaced electron gas and electromagnetic coupling among neighboring nanoparticles, which leads to a shorter resonance wavelength.

In another work of Hyung Ju Kim et al [19] size-controllable Au nanodot arrays (height of nanodot 12-15 nm) on Ti adhesion layer (ca. 1 nm) are directly printed onto indium tin oxide (ITO) glasses and then coated with TiO_2 layer (110 nm in thickness) by dip-coating followed by annealing process at 300^oC. Experimentally has been shown that the plasmon resonance wavelength (λ_{LSPR}) experiences a redshift as the Au nanodot size (or length) increases from 50 nm to 83 nm (Fig. 4 a). Increasing the gap (at the same time decreasing the size or length

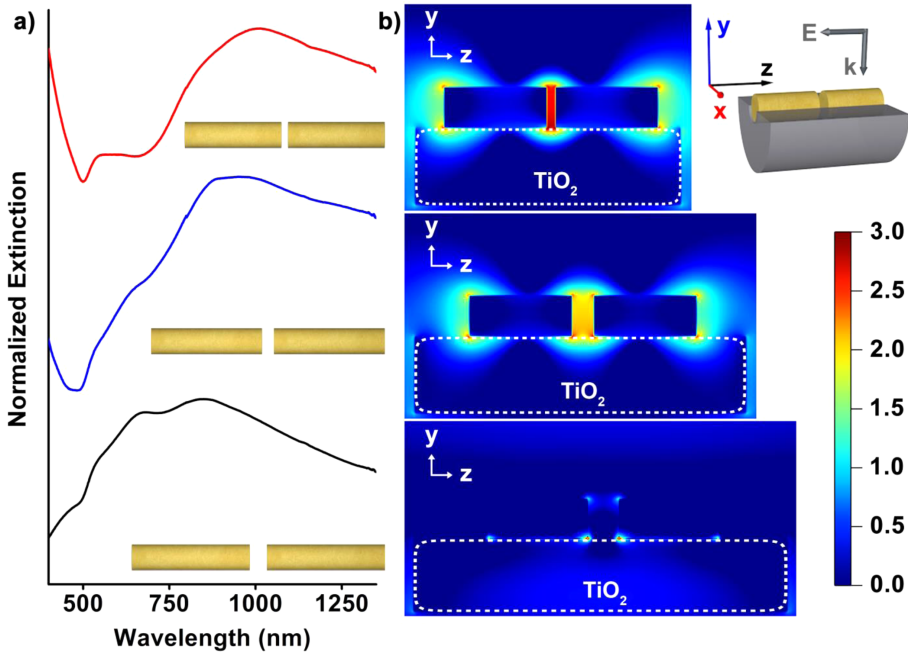

Fig. 2. (a) Normalized UV-vis-NIR spectra for plasmonic dimers with differing gap sizes embedded in sheets of anatase TiO_2 in water. (b) FDTD electric field intensity maps of gold nanorod dimers that are 43 nm in diameter, have gaps between dimer segments of 7, 18, and 28 nm, and are coated with a half shell of 80 nm thick anatase TiO_2 (see inset) [17].

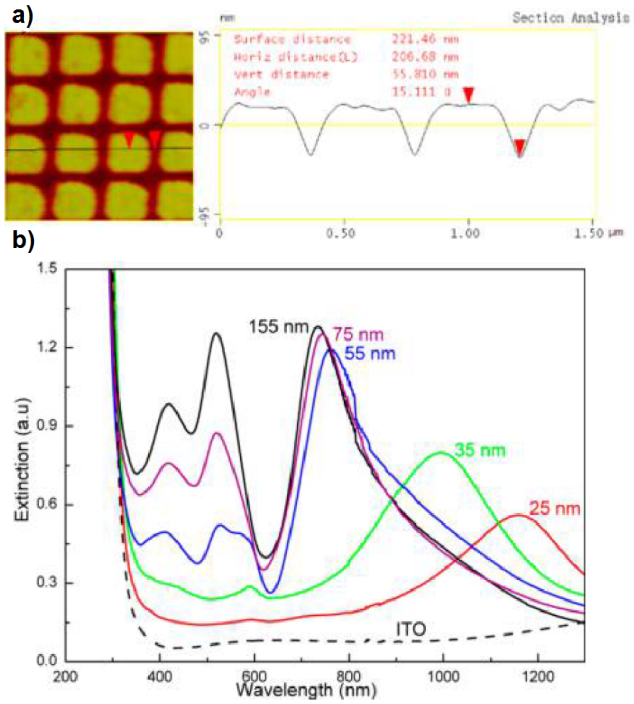

Fig. 3. (a) AFM section analyses of Au nanoparticles with heights of about 55 nm; (b) Experimental UV-vis-NIR extinction spectra of Au nanoparticle arrays deposited on ITO-coated glasses with heights of about 25, 35, 55, 75, and 155 nm [11].

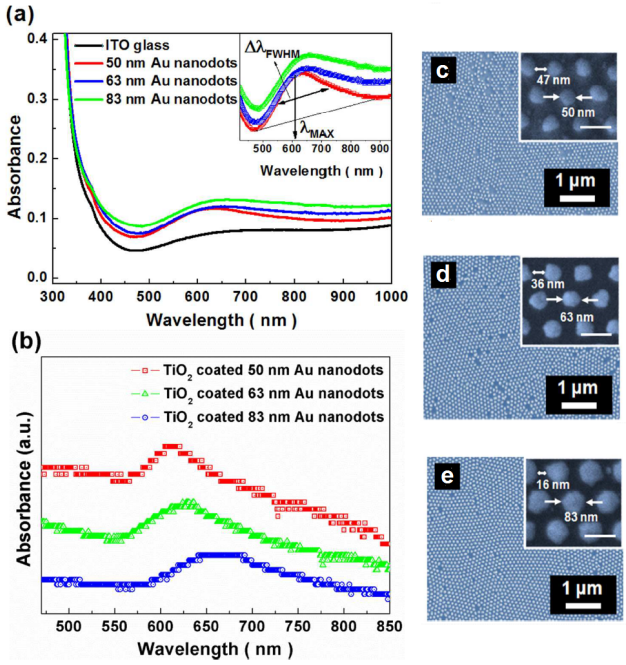

Fig. 4. (a) UV-Vis absorption spectra of 50 nm, 63 nm and 83 nm Au nanodots on ITO glass. (b) UV-Vis absorption spectra of TiO_2 coated 50 nm, 63 nm and 83 nm Au nanodots on ITO glass. The Figure shows difference spectra for Au nanodots (i.e., the spectrum of TiO_2 coated Au nanodots on ITO glass minus the spectrum of TiO_2 coated ITO glass). (c-e) SEM images of prepared Au nanodot arrays [19].

(Fig. 4 c-e)) between nanodots we can see blue shift (Fig. 4 a, b) and decrease in absorbance (for bare gold).

But not all possible structures of the gold topography could be interpreted as arrays of monopoles and dimers. Another way of designing gold topography was proposed by Alyssa J. Pasquale et al. [16] where thanks to the E-beam lithography were formed concentric necklace nanolenses which consist of metal nanoparticle dimers placed in the center of one or more concentric rings of plasmonic necklaces. The introduction of concentric rings around metal nanodisk dimers significantly concentrates the electric field at the gap within the dimer region. The intensity of the electric field increases as the number of necklaces increases, as shown in the FDTD simulations presented in (Fig. 5).

In work of Bouvree et al. [15] by E-beam nanolithography, two kinds of patterns, lines and circles were formed from Au nanoparticles with fixed size of 22 nm (Fig. 6 b,c). The interline and inter-circle distances were set from 20 to 2000 nm. Two line thickness values, 30 and 60 nm, had been achieved, corresponding to bands of two or three AuNP widths. It should be pointed here that "line"patterns were sensitive to the light polarization, whereas "circle"patterns were nonsensitive. Signals recorded on concentric rings were lower than observed for lines. (Fig. 6 a) displays experimental Raman scattering results obtained on various patterns. The intensity (counts/s) of the band at $1,620cm^{-1}$ (crystal violet) is reported as a function of the distance between lines.

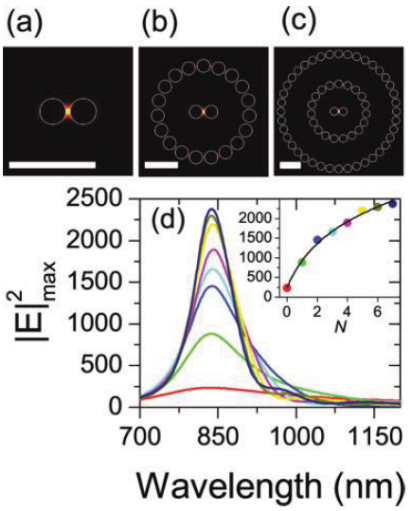

Fig. 5. Calculated near-field intensity distributions at 785 nm of (a) isolated dimer, (b) dimer/enneadecagon, and (c) dimer/ enneadecagon/tetracontagon. Scale bars correspond to 500 nm. (d) Near-field intensity spectra of an isolated dimer (red) embedded into optimized single (green), double (blue), triple (blue), through seven (navy) necklace(s). Inset shows the evolution of the maximum near-field intensity with the number of surrounding necklaces, N, fitted to a logarithmic function [16].

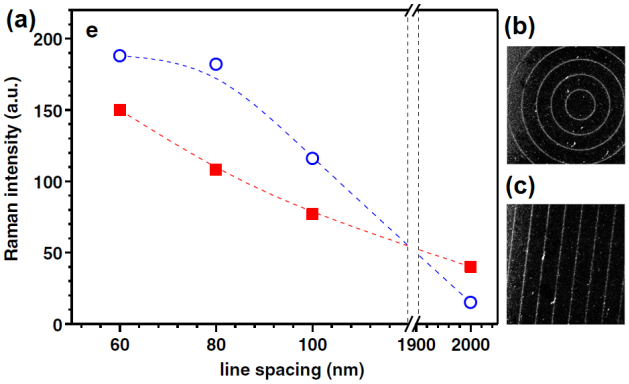

Fig. 6. (a) Comparison of the Raman intensity measured for the band of crystal violet at $1,620cm^{-1}$ as a function of the distance between AuNPs lines (square : 30 nm width ofthe line, circle : 60 nm width of the lines). (b and c) SEM images of immobilized AuNPs on nanopatterned substrates [15].

3 Dielectric oxide materials

From practical application viewpoint, not only strong enhancement but also stability, recyclability as well as cost-effective preparation methods are necessary for SERS sensors productivity. To this end, the fabrication of SERS-active substrates with optimized properties is still faced with numerous challenges. Because of the mixture among metal nanoparticles, solutions and target molecules, the nanoparticle metal surface influenced by the adhesion of solutions and target molecules, thereby influencing the accuracy of the Raman spectra of the target molecule.

To reduce these errors and incorporate new functionalities, these plasmonic metal nanoparticles have been coupled with various dielectric oxide materials (e.g., SiO_2 [12,20], TiO_2 [10], Al_2O_3 [21] etc.) to form metal-oxide hybrid nanostructures and prevent contact between the metal surfaces and target molecules. For example in work of Lingwei Ma et al [22] slanted silver nanorodes were prepared on oblique angle vapor deposition (OAD) technique and then covered with different TiO_2 layers thicknesses using atomic layer deposition (ALD) (each ALD cycles added 0.55 nm of TiO_2 thickness). (Fig 7 a) shows influence of the covering layer thicknesses on the output intensity of the Raman signal from 10^{-5} M crystal violet molecules. Also temporal stability of bare Ag and $Ag@TiO_2$ NRs was supervised via counting the SERS intensities of 10^{-5} M CV from the stored substrates as a function of time. (Fig 7 b) displays the normalized Raman intensities at 1171 cm^{-1} band obtained from different substrates over a period of 48 days. As can been seen, CV signals on bare Ag NRs emerged a substantial decline even only after 8 days (50% drop), and were more than one order smaller after 48 days. However, when the NRs were uniformly wrapped with ultrathin TiO_2, their

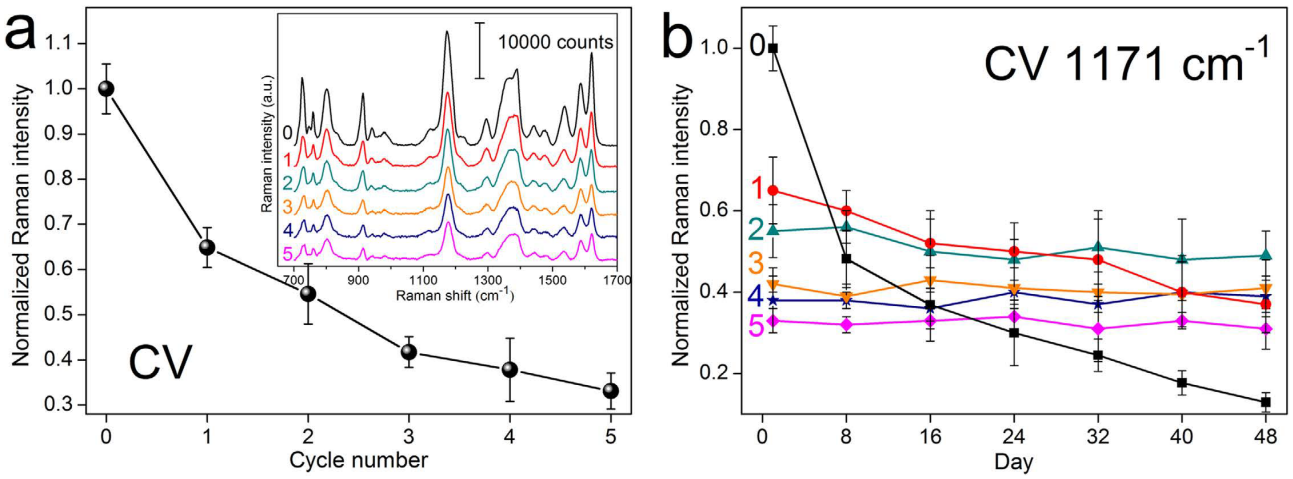

Fig. 7. (a) The normalized Raman intensities of 1171 cm^{-1} peak from 10^{-5} M CV molecules versus the atimic layer deposition (ALD) cycles of $Ag@TiO_2$ NRs. The inset illustrates the Raman spectra of 10^{-5} M CV adsorbed on bare Ag NRs and $Ag@TiO_2$-1 (0.55 nm thickness of TiO_2), $Ag@TiO_2$-2 (1.1 nm), $Ag@TiO_2$-3 (1.65 nm), $Ag@TiO_2$-4 (2.2 nm), $Ag@TiO_2$-5 (2.75 nm) NRs, respectively. (b) The normalized Raman intensities of 1171 cm^{-1} peak on these substrates during aging in air for 48 days [22].

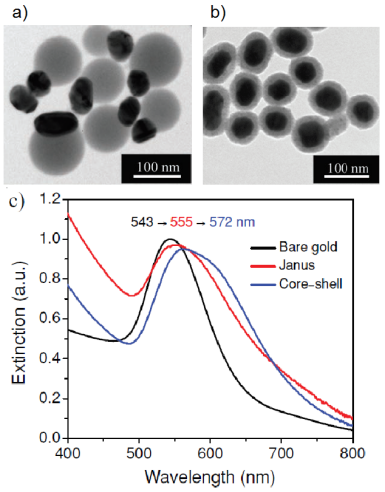

Fig. 8. (a,b) TEM images of Janus(a) and core-shell(b) $Au@TiO_2$ nanostructures. (c) Optical-extinction spectra of bare gold NPs (50 nm in diameter), as well as Janus and core-shell $Au@TiO_2$ nanostructures in isopropyl alcohol, which were taken from experimental measurements [10].

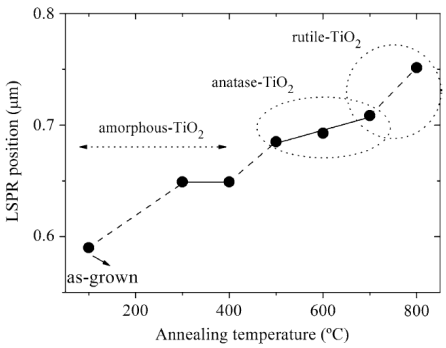

Fig. 9. Evolution of the LSPR peak position as a function of the annealing temperature of TiO_2 host matrix with embedded gold NPs [26].

stability was dramatically enhanced.

Adding new material also change combined optical, electronic and magnetic properties. Via depositing high optical index of refraction film on metal surface we can tune the LSPR peak position [23]. Increase in the refractive index of the dielectric environment that surrounds the plasmonic metal nanoparticle causes red shift in LSPR peak position [10, 12, 21, 23]. Even the covering deposition technique, the way of covering [10] (Fig 8 a,b), sequence in which this oxide material was added [24, 25], annealing temperature with which material was treated [26] (Fig 9), thickness of this additional layer [21–23, 27] has an influence on the final SERS activity.

In this study we compare two materials for protective covering shell: SiO_2 and TiO_2. The task is to decide which material to use and what parameters it has to have to produce the best SERS results. Looking at the previous results [21, 27] we can assume that thickness changing of SiO_2 shell with the Au core even on 1 nm can dramatically damp the scattered signal (Fig 11) (minus 1 order of electric field magnitude from 1 nm to 2 nm thickness of covering layer). On the figure below we can see that SiO_2 as covering layer material is very sensitive to the thickness variation. So it would be difficult to produce the same substrates with the same properties without any changes in a layer thickness, even on 1 nm.

In the work of Sergey Scherbak et al. [23] were tested different thicknesses of TiO_2 layer on a gold films (Fig. 10). Was determined optimal thickness of TiO_2 covering

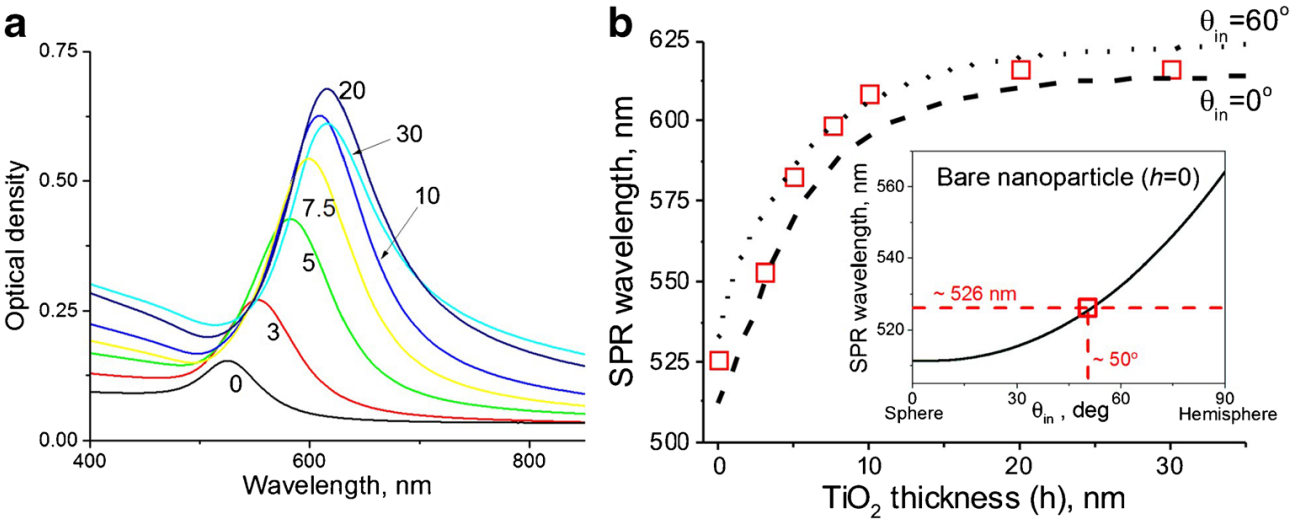

Fig. 10. (a) Absorption spectra of gold nanoisland films coated with TiO_2 films of different thicknesses (thickness in nanometer marked near the curves). Before coating, all the samples were annealed at 500 ^oC for 120 min. (b) Experimental (squares) and theoretical thickness dependencies of the surface plasmon resonance wavelength. Theoretical results are presented for truncated gold nanospheres with different truncation angles θ_{in}. Inset: spectral position of the SPR wavelength as a function of bare nanosphere truncation angle, the square marker denotes the measured wavelength of the SPR [23].

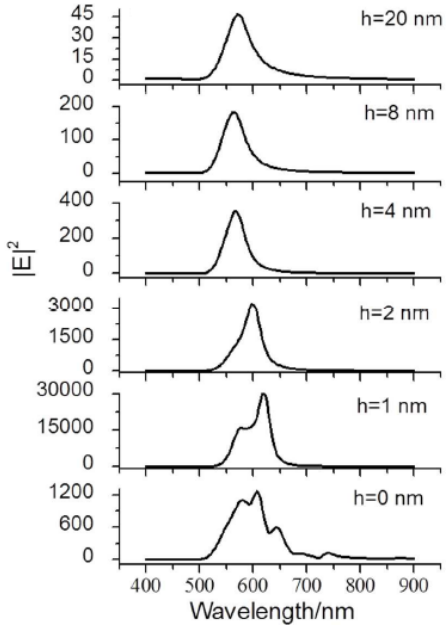

Fig. 11. The electric field enhancements of Au NP with the diameter 80 nm for different thicknesses of SiO_2 shell [27].

layer (about 20-30 nm for a truncated gold nanospheres of 8.8 nm in radius on the glass substrate), where the induced electric field is almost fully localized in the covering layer and the particle barely "feels"any further increase in the coating thickness. It was demonstrated that the λ_{LSPR} can be precisely shifted up to 100 nm towards longer wavelengths by depositing titania layer on the island film. So we can conclude that the thickness changing of TiO_2 material as covering layer is not so crutial for the final enhancement.

Another way to study the enhancement mechanism in such bilayer thin films is submit these substrates as photoelectrodes. With this approach we can characterize the enhancing mechanism throught photoconversion in metal-semiconductor heterojunction-based photovoltaics and photocatalysts.

In metal-semiconductor heterojunctions, the plasmon is able to induce charge separation in the semiconductor via three mechanisms: (i) photonic enhancement, (ii) direct electron transfer (DET) also known as hot electron injection, and (iii) plasmon-induced resonance energy transfer (RET) [3, 24, 28].

For the photonic enhancement, the plasmon can interact with the semiconductor by far-field radiation, improving light absorption in the semiconductor via light trapping. It can happen only when the incident photon's energy is larger than the band gap of the semiconductor [3].

For DET, the nonthermalized electrons excited by a localized surface plasmon resonance (LSPR) have energy above that of the Fermi level in the metal, allowing the Schottky barrier created by charge equilibrium between the metal and the semiconductor to be overcome in the excited state [29]. Thus the electron transfer process does not require the energetically favorable equilibrium band alignment.

On (Fig. 12) illustrated the scheme of these electron transfers. The gold core converts the energy of incident photons into localized surface plasmon resonance oscillations and transfers the plasmonic energy to the TiO_2 semiconductor shell via resonant energy transfer.

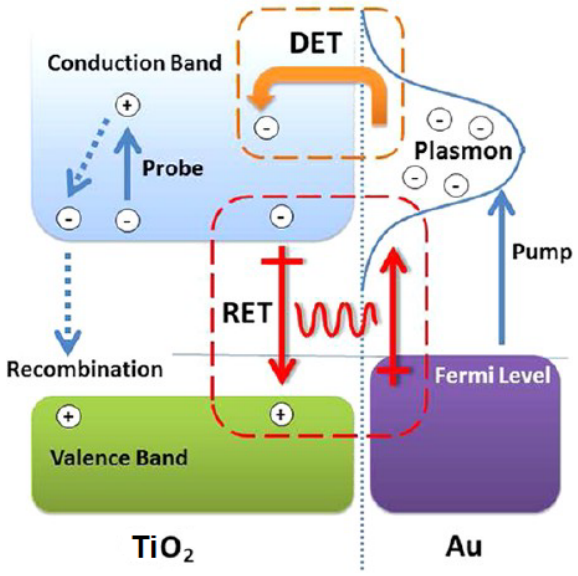

Fig. 12. After excitation of the plasmon by the pump laser the plasmon can enhance carrier creation in the TiO_2 by hot electron injection or plasmon-induced RET [28].

RET generates electron-hole pairs in the semiconductor by the dipole-dipole interaction between the plasmonic metal (donor) and semiconductor (acceptor), which greatly enhances the visible-light photocatalytic activity as compared to the semiconductor alone [28].

In the work of Scott K. Cushing et al. [3] nanospheres of gold (50 nm in diameter) were covered with 10 nm of SiO_2 and then with 20 nm of TiO_2. Transient absorption spectroscopy was chosen to experimentally determine the plasmonic enhancement mechanism, since it allows the transfer and creation of carriers to be measured on a picosecond time scale, before recombination can reduce the carrier population. It has been found that SiO_2 serves as an insulating barrier, whose 10 nm thickness is sufficient to block hot electron transfer but still allowed coupling through the plasmon's near field.

As for TiO_2 layer, it was found some interesting properties. In the work of Hongjun Chen et al [24] only by switching the deposition sequence of the TiO_2 layer on a simple bilayer structure of 5 nm thick Au and 10 nm TiO_2 on fluorine-doped tin oxide (FTO) as a substrate (Fig. 13), it is possible to change the photocurrent direction under visible-light irradiation. It is found that when Au layer is deposited as the outer layer on TiO_2 coated FTO substrate, an anodic photocurrent is obtained due to the band bending formed at the electrode-electrolyte interface. But when Au is under TiO_2 layer the cathodic photocurrent appears.

Here photogenerated electrons can be easily trapped in the energy well formed between the band bending and the Schottky contact, which allows electronic tunnelling through the 1.6 nm thick space charge layer, resulting in

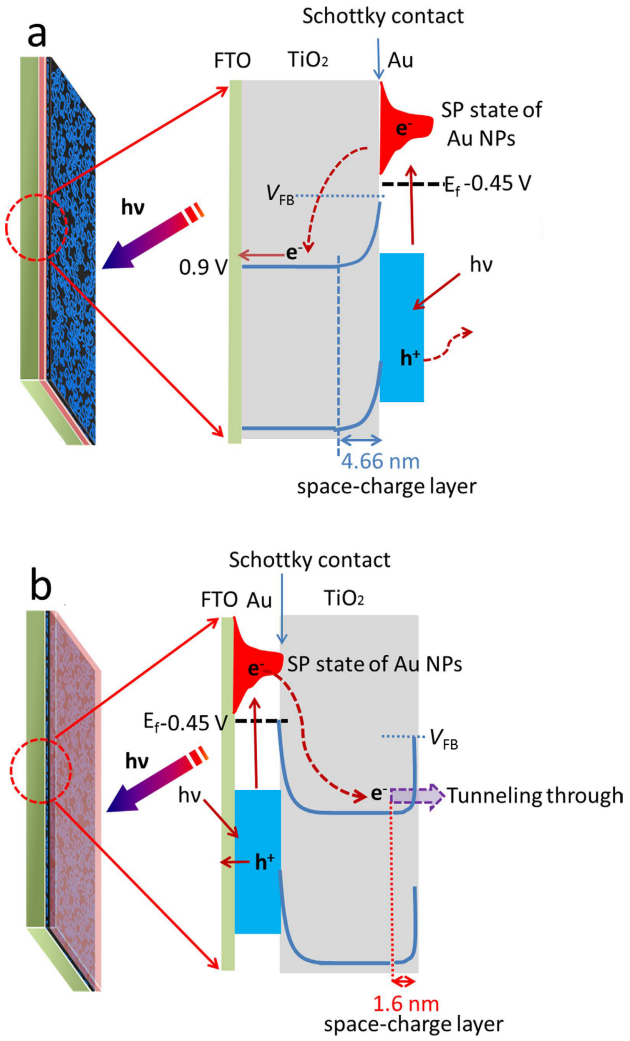

Fig. 13. Schematic illustration of the visible-light excited charge-transferred process for Au/TiO_2 bilayer structures: (a) $FTO/TiO_2/Au$ and (b) $FTO/Au/TiO_2$; here V_{FB} = Flat-band potential, E_f = Femi level [24].

a unique anodic to cathodic photocurrent conversion.

For our task cathodic photocurrent is more desirable since the generated photovoltage under visible illumination are totally changed into positive values, suggesting positive charges are accumulated at the surface. If the TiO_2 layer of $FTO/Au/TiO_2$ photoelectrode increases to 100 nm, the thus-obtained photoelectrode still keeps cathodic photocurrent [24], suggesting the tunnelling effect still exists, not being dependence of the thickness of TiO_2 layer.

It is also worth to mention work of Hyung Ju Kim et al [19] where has been found that the activity of each catalyst (Au nanodot array with different sizes on Ti adhesion layer on ITO substrate) increased by a factor

of 6 times when 110 nm of TiO_2 was added to the Au nanodots for all samples.

Conclusion

Over the past four decades, since the discovery of SERS, a series of theoretical and technological innovations have stimulated broad interest in plasmonic nanomaterials. This review was devoted to the analysis of the of the latest research on the elucidation of occurrence of Raman signal enhancement mechanisms. At the beginning the reader was introduced to the SERS phenomenon. Then it was said why it is better choose gold for a role as a plasmonic metal over silver. The function of sensor's recyclability and stability with two oxide materials SiO_2 and TiO_2 were analysed. It has been found that change of upper protective layer thickness in case of TiO_2 at 1 or 2 nm is not so crutial as for SiO_2. This allows the production of sensors with less precision, and hence cost. The main trends in the signal change were considered depending on changes in individual parameters of the nanostructure in order to determine the optimal topography of the metal surface.

References

[1] Guillot N. and Lamy M. (2012) The electrolatexcompanionmagnetic effect in surface enhanced Raman scattering: Enhancement optimization using precisely controlled nanostructures, *J of Quantitative Spectroscopy and Radiative Transfer*, Vol. 113, Is. 18, pp. 2321-2333.

[2] Yoon J., Dong J., Sung-Gyu P., Shin-Hyun K. and Dong-Ho K. (2016) Nanostructured plasmonic substrates for use as SERS sensors, *Nano Convergence*, Vol. 3, No.1, 18p.

[3] Cushing K., Li J., Bright J., Yost B., Zheng P., Bristow A. and Nianqiang W. (2015) Controlling Plasmon-Induced Resonance Energy Transfer and Hot Electron Injection Processes in Metal@TiO2 Core-Shell Nanoparticles, *J. Phys. Chem. C*, Vol. 119 (28), pp 16239–16244.

[4] Katherine Willets A. and Richard P. (2007) Localized Surface Plasmon Resonance Spectroscopy and Sensing, Annu. Rev. Phys. Chem., Vol. 58, pp. 267-297.

[5] Hakonen A., Svedendahl M., Ogier R., Yang Z., Lodewijks K., Verre R., Shegai T., Anderssonb P. and Kall M. (2015) Dimer-on-mirror SERS substrates with attogram sensitivity fabricated by colloidal lithography, *Nanoscale*, Vol. 7, No. 21, pp. 9405-9410. DOI: 10.1039/c5nr01654a

[6] Hyunhyub K., Chang S. and Vladimir V. (2009) Porous Substrates for Label-Free Molecular Level Detection of Nonresonant Organic Molecules. *ACS Nano*, Vol. 3, pp. 181-188. DOI: 10.1021/nn800569f

[7] Etchegoin P., Le Ru E., and Meyer M. (2006) An analytic model for the optical properties of gold, *J. Chem. Phys.*, Vol. 125, pp. 164705. DOI: 10.1063/1.2360270

[8] Yu-LuenDeng, Yi-JeJuang (2014) Black silicon SERS substrate: Effect of surface morphology on SERS detection and application of single algal cell analysis, *Biosensors and Bioelectronics*, Vol. 53, pp. 37-42. DOI: 10.1016/j.bios.2013.09.032

[9] Chen J., Yinyong Li, Huang K., Wang P., He L., Carter K., and Nugen S. (2015) Nanoimprinted Patterned Pillar Substrates for Surface-Enhanced Raman Scattering Applications, *ACS Appl. Mater. Interfaces*, Vol. 7, pp. 22106-22113. DOI: 10.1021/acsami.5b07879

[10] Zhi Wei Seh, Shuhua Liu, Michelle Low, Shuang-Yuan Zhang, Zhaolin Liu, Adnen Mlayah, and Ming-Yong Han (2012) Janus Au-TiO 2 Photocatalysts with Strong Localization of Plasmonic Near-Fields for Effi cient Visible-Light Hydrogen Generation, *Advanced Materials*, Vol. 24, No 17, pp. 2310-2314. DOI: 10.1002/adma.201104241

[11] Zhibing Zhan, Rui Xu, Yan Mi, Huaping Zhao, and Yong Lei (2015) Highly Controllable Surface Plasmon Resonance Property by Heights of Ordered Nanoparticle Arrays Fabricated via a Nonlithographic Route, *ACS Nano*, Vol. 9, No. 4, pp. 4583-4590. DOI: 10.1002/adma.201104241

[12] Quyen T., Chang C., Su W., Yih-Huei Uen, Pan C., Liu J., Rick J., Lin K. and Hwang B. (2014) Self-focusing Au@SiO2 nanorods with rhodamine 6G as highly sensitive SERS substrate for carcinoembryonic antigen detection, *J. Mater. Chem. B*, Vol. 2, pp. 629. DOI: 10.1039/c3tb21278e

[13] Kozanoglu D., Apaydin D., Cirpan A., Esenturk E. (2013) Power conversion efficiency enhancement of organic solar cells by addition of gold nanostars, nanorods, and nanospheres, *Organic Electronics*, Vol. 14, pp. 1720-1727. DOI: http://dx.doi.org/10.1016/j.orgel.2013.04.008

[14] Niu W., Chua Y., Zhang W., Huang H. and Lu X. (2015) Highly Symmetric Gold Nanostars: Crystallographic Control and Surface-Enhanced Raman Scattering Property, *J. Am. Chem. Soc.*, Vol. 137 (33), pp. 10460-10463. DOI: 10.1021/jacs.5b05321

[15] Bouvree A., D'Orlando A., Makiabadi T., Martin S., Louarn G., Mevellec J. and Humbert B. (2013) Nanostructured and nanopatterned gold surfaces: application to the surface-enhanced Raman spectroscopy, *Gold Bull*, Vol. 46, pp. 283-290. DOI: http://dx.doi.org/10.1007/s13404-013-0127-4

[16] Alyssa J., Bjorn M. Reinhard and Luca Dal Negro (2012) Concentric Necklace Nanolenses for Optical Near-Field Focusing and Enhancement, *ACS Nano*, Vol. 6 (5), pp. 4341-4348. DOI: 10.1021/nn301000u

[17] Mangelson B., Jones M., Park D., Shade C., Schatz G. and Mirkin C. (2014) Synthesis and Characterization of a Plasmonic−Semiconductor Composite Containing Rationally Designed, Optically Tunable Gold Nanorod Dimers and Anatase TiO_2, *ACS Chem. Mater.*, DOI: http://dx.doi.org/10.1021/cm5014625

[18] Mousavi S., Berini P. and McNamara D. (2012) Periodic plasmonic nanoantennas in a piecewise homogeneous background, *OSA Optics Express*, Vol. 20 (16), pp. 18044-18065. DOI: 10.1364/oe.20.018044

[19] Kim H., Lee S., Upadhye A., Insoo Ro, Tejedor-Tejedor I., Anderson M., Kim W. and Huber G. (2014) Plasmon-Enhanced Photoelectrochemical Water Splitting with Size-Controllable Au Nanodot Arrays, *ACS Nano*. DOI: http://dx.doi.org/10.1021/nn504484u

[20] Ruoping L., Guanghong Y., Jingliang Y., Junhe H., Junhui L. and Mingju H. (2016) Determination of melamine in milk using surface plasma effect of aggregated Au@SiO2 nanoparticles by SERS technique, *Food Control*, Vol. 68, pp. 14-19. DOI: http://dx.doi.org/10.1016/j.foodcont.2016.03.009

[21] Kuo H. and Chang C. (2014) Analysis of Core-Shell-Isolated Nanoparticle Configurations Used in the Surface-Enhanced Raman Scattering Technique, *J. IEEE Sensors*, Vol. 14, No 10, pp. 3708-3714. DOI: 10.1109/jsen.2014.2331459

[22] Lingwei M., Huang Y., Mengjing H., Xie Z. and Zhang Z. (2015) Ag Nanorods Coated with Ultrathin TiO2 Shells as Stable and Recyclable SERS Substrates, *Sci. Rep.*, Vol. 5, pp. 15442. DOI: http://dx.doi.org/10.1038/srep15442

[23] Scherbak S., Kapralov N., Reduto I., Chervinskii S., Svirko O. and Lipovskii A. (2016) Tuning Plasmonic Properties of Truncated Gold Nanospheres by Coating, *Springer Science+Business Media New York*. DOI: 10.1007/s11468-016-0461-5

[24] Chen H., Liu G., Wang L. (2105) Switched photocurrent direction in Au/TiO2 bilayer thin films, *Sci. Rep.*, Vol. 5, No. 1, pp. 10852. DOI: 10.1038/srep10852

[25] Zhan Z., An J., Zhang H., Hansen R. and Zheng L. (2014) Three-Dimensional Plasmonic Photoanodes Based on Au-Embedded TiO2 Structures for Enhanced Visible-Light Water Splitting, *ACS Appl. Mater. Interfaces*, Vol. 6, 1139-1144. DOI: 10.1021/am404738a

[26] Borges J., Buljan M., Sancho-Parramon J., Bogdanovic-Radovic I., Siketic Z., Scherer T., Kubel C., Bernstorff S., Cavaleiro A., Vaz F., Rolo A. (2014) Evolution of the surface plasmon resonance of Au-TiO2 nanocomposite thin films with annealing temperature, *J Nanopart Res*, Vol. 16, 2790. DOI: 10.1007/s11051-014-2790-7

[27] Chen S., Yang Z., Meng L., Li J., Williams C., and Tian Z. (2015) Electromagnetic Enhancement in Shell-Isolated Nanoparticle Enhanced Raman Scattering from Gold Flat Surfaces, *J. Phys. Chem. C.* DOI: 10.1021/acs.jpcc.5b01254

[28] Cushing S., Li J., Meng F., Senty T., Suri S., Zhi M., Li M., Bristow A., and Wu N. (2012) Photocatalytic Activity Enhanced by Plasmonic Resonant Energy Transfer from Metal to Semiconductor, *J. Am. Chem. Soc.*, Vol. 134, 15033-15041. DOI: 10.1021/ja305603t

[29] Li J., Cushing S., Bright J., Meng F., Senty T., Zheng P., Bristow A., and Wu N. (2013) $Ag@Cu_2O$ Core-Shell Nanoparticles as Visible-Light Plasmonic Photocatalysts, *ACS Catal.*, Vol. 3, 47-51. DOI: 10.1021/cs300672f

Розробка наноструктурованих плазмонних підкладок для використання в якості датчиків ГКР

Банделюк О. В., Колобродов В. Г.

Плазмонні наноструктури сильно локалізують електричне поле на їх поверхнях за допомогою колективних коливань електронів провідності при стимуляції падаючим світлом на певній довжині хвилі. Молекули, адсорбовані на таких поверхнях, відчувають сильно посилене електричне поле через локалізований поверхневий плазмонний резонанс (ЛППР), який підсилює сигнал комбінаційного розсіювання від цих молекул. Це явище називають поверхневим гігантським комбінаційним розсіюванням (ГКР). Подальші поліпшення в інтенсивності комбінаційного розсіювання були досягнуті шляхом проектування плазмонних наноструктур з контрольованим розміром, формою, складом та розташуванням. У цій оглядовій статті основна увага приділяється теорії та аналізу впливу захисного покриття на оксидні матеріали на ізольовані наноструктури плазмонних металів. Починаючи з короткого опису основних принципів, що лежать в основі ЛППР і ГКР, ми порівнюємо два плазмонних метала, два діелектричних матеріала і вплив зміни окремих параметрів наноструктури на вихідний посилений сигнал комбінаційного розсіювання.

Ключові слова: ГКР; плазмон; молекула; гетероперехід метал-напівпровідник; наноструктура

Разработка наноструктурированных плазмонных подложек для использования в качестве датчиков ГКР

Банделюк А. В., Колобродов В. Г.

Плазмонные наноструктуры сильно локализуют электрическое поле на их поверхностях посредством коллективных колебаний проводящих электронов при стимуляции падающим светом на определенной длине волны. Молекулы, адсорбированные на таких поверхностях, испытывают сильно усиленное электрическое поле из-за локализованного поверхностного плазмонного резонанса (ЛППР), который усиливает сигнал комбинационного рассеяния от этих молекул. Это явление называют поверхностным гигантским комбинационным рассеянием (ГКР). Дальнейшие улучшения в интенсивности комбинационного рассеяния были достигнуты путем проектирования плазмонных наноструктур с контролируемым размером, формой, составом и расположением. В этой обзорной статье основное внимание уделяется теории и анализ у влияния защитного покрытия на оксидные материалы на изолированные наноструктуры плазмонных металлов. Начиная с краткого описания основных принципов, лежащих в основе ЛППР и ГКР, мы сравниваем два плазмонных металла, два диэлектрических материала и влияние изменения отдельных параметров наноструктуры на выходной усиленный сигнал комбинационного рассеяния.

Ключевые слова: ГКР; плазмон; молекула; гетероперехід металл-полупроводник; наноструктура